

Alteration of the Substrate Specificity of the Angular Dioxygenase Carbazole 1,9a-Dioxygenase

Hiromasa UCHIMURA,^{1,*,**} Tadafumi HORISAKI,^{1,2,*} Takashi UMEDA,¹ Haruko NOGUCHI,^{1,3} Yusuke USAMI,¹ Li LI,^{1,***} Tohru TERADA,^{3,****} Shugo NAKAMURA,⁴ Kentaro SHIMIZU,^{3,4} Tetsuo TAKEMURA,² Hiroshi HABE,^{1,*****} Kazuo FURIHATA,⁵ Toshio OMORI,^{1,*****} Hisakazu YAMANE,¹ and Hideaki NOJIRI^{1,3,†}

¹Biotechnology Research Center, The University of Tokyo, 1-1-1 Yayoi, Bunkyo-ku, Tokyo 113-8657, Japan

²Department of Chemistry, Faculty of Science, Tokyo University of Science, 1-3 Kagurazaka, Shinjuku-ku, Tokyo 162-8601, Japan

³Professional Program for Agricultural Bioinformatics, The University of Tokyo, 1-1-1 Yayoi, Bunkyo-ku, Tokyo 113-8657, Japan

⁴Department of Biotechnology, The University of Tokyo, 1-1-1 Yayoi, Bunkyo-ku, Tokyo 113-8657, Japan

⁵Department of Applied Biological Chemistry, The University of Tokyo, 1-1-1 Yayoi, Bunkyo-ku, Tokyo 113-8657, Japan

Received July 28, 2008; Accepted August 27, 2008; Online Publication, December 7, 2008
[doi:10.1271/bbb.80512]

Carbazole 1,9a-dioxygenase (CARDO) consists of terminal oxygenase (CARDO-O) and electron transport components. CARDO can catalyze specific oxygenation for various substrates: angular dioxygenation for carbazole and dibenzo-*p*-dioxin, lateral dioxygenation for anthracene, and monooxygenation for methylene carbon of fluorene and sulfide sulfur of dibenzothiophene. To elucidate the molecular mechanism determining its unique substrate specificity, 17 CARDO-O site-directed mutants at amino acid residues I262, F275, Q282, and F329, which form the substrate-interacting wall around the iron active site by CARDO-O crystal structure, were generated and characterized. F329 replacement dramatically reduced oxygenation activity. However, several mutants produced different products from the wild-type enzyme to a large extent: I262V and Q282Y (1-hydroxycarbazole), F275W (4-hydroxyfluorene), F275A (unidentified *cis*-dihydrodiol of fluoranthene),

and I262A and I262W (monohydroxydibenzothiophenes). These results suggest the possibility that the respective substrates bind to the active sites of CARDO-O mutants in a different orientation from that of the wild-type enzyme.

Key words: angular dioxygenation; carbazole 1,9a-dioxygenase; Rieske non-heme iron oxygenase; site-directed mutagenesis; substrate specificity

Metabolically versatile bacteria play an important role in decomposing released aromatic compounds regardless of their origin. Although sufficient induction time is occasionally needed to detect degradation, most natural and synthetic aromatic compounds are mineralized or partially converted to other compounds. Aerobic degradation of various aromatics, including toxic solvents,

† To whom correspondence should be addressed. Fax: +81-3-5841-8030; E-mail: anojiri@mail.ecc.u-tokyo.ac.jp

* These two authors contributed equally to this work.

** Present address: Laboratory of Proteomic Sciences, 21st Century COE Program, Kyoto Pharmaceutical University, Yamashina-ku, Kyoto 607-8412, Japan

*** Present address: School of Environmental Science and Engineering, Shandong University, Jinan 250100, People's Republic of China

**** Present address: Computational Science Research Program, RIKEN, 2-1 Hirosawa, Wako, Saitama 351-0198, Japan

***** Present address: National Institute of Advanced Industrial Science and Technology (AIST), Central 5-2, 1-1-1 Higashi, Tsukuba, Ibaraki 305-8565, Japan

***** Present address: Department of Industrial Chemistry, Shibaura Institute of Technology, 3-9-14 Shibaura, Minato-ku, Tokyo 108-8548, Japan

Abbreviations: AD, angular dioxygenation; Ap, ampicillin; BDO, biphenyl 2,3-dioxygenase; BDO-O, terminal oxygenase component of BDO; CARDO, carbazole 1,9a-dioxygenase; CARDO-F, ferredoxin component of CARDO; CARDO-O, terminal oxygenase component of CARDO; CARDO-R, ferredoxin reductase component of CARDO; GC-MS, gas chromatography-mass spectrometry; HPLC, high-performance liquid chromatography; LD, lateral dioxygenation; MSTFA, *N*-methyl-*N*-trimethylsilyltrifluoroacetamide; NDO, naphthalene 1,2-dioxygenase; NDO-O, terminal oxygenase component of NDO; NMR, nuclear magnetic resonance; PCB, polychlorinated biphenyl; RO, Rieske non-heme iron oxygenase; SDS-PAGE, sodium dodecyl sulfate-polyacrylamide gel electrophoresis; TLC, thin-layer chromatography; WT, wild type

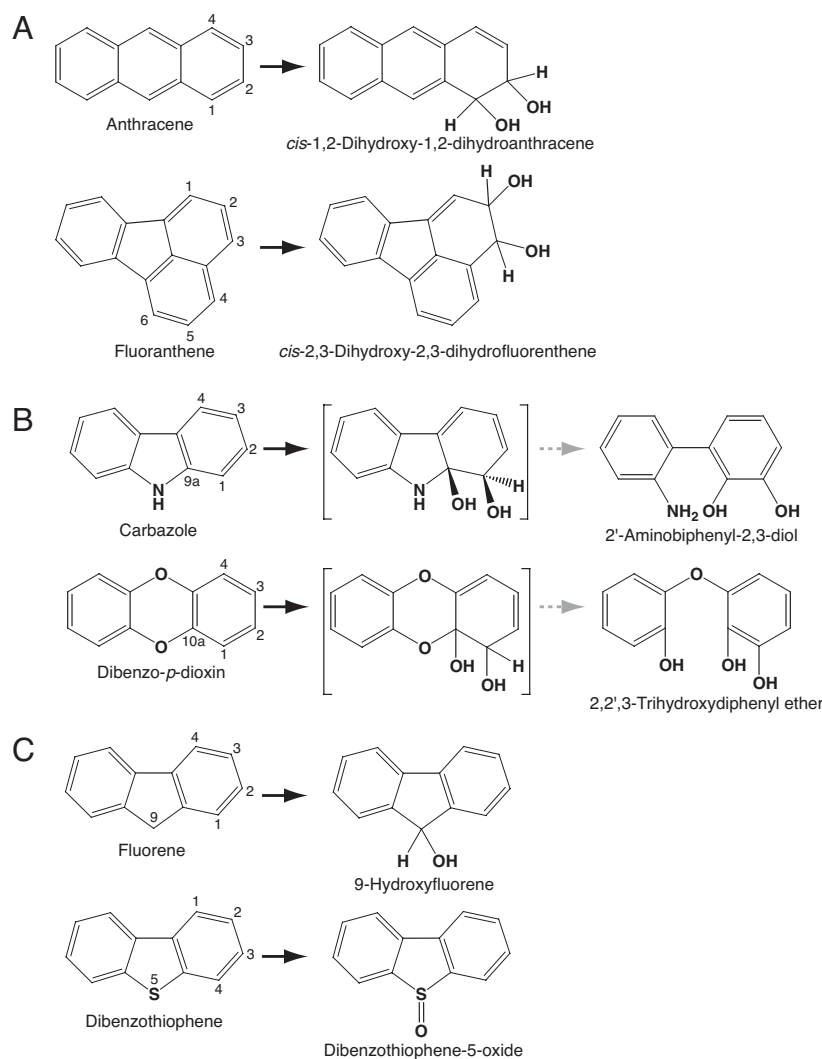


Fig. 1. Diverse Types of Oxygenation Catalyzed by CARDO.

CARDO catalyzes *cis*-dihydroxylation at lateral positions (lateral dioxygenation, LD) for anthracene and fluoranthene (A), *cis*-dihydroxylation at angular positions (angular dioxygenation, AD) for carbazole and dibenzo-*p*-dioxin (B), and monooxygenation for methylene carbon of fluorene and sulfide sulfur of dibenzothiophene (C). Only the main products are shown for the respective substrates. Absolute stereochemistry is not intended, with the exception of the AD product of carbazole (1,9a-dihydroxy-1-hydrocarbazole), for which the stereochemistry is proposed based on the carbazole-bound structure at the active site of CARDO-O.¹¹⁾ The oxygenation products shown in brackets are unstable and were not detected directly.

agrochemicals, medicines, and industrial raw materials, is a key phenomenon in removing previously released contaminants from subsurface areas such as surface soils, river water, and seashores. Compared with anaerobic bacterial degradation, aerobic bacterial degradation generally progresses more rapidly because of the enhanced metabolic status, and has been studied for various xenobiotic compounds to provide basic information on its potential use in the removal of aromatic contaminants from the environment.

Bacterial metabolism of aromatic compounds is usually initiated by dioxygenation catalyzed by Rieske non-heme iron oxygenase (RO). RO members are multicomponent-type enzymes that consist of terminal oxygenase and electron transfer components. RO members constitute an important class of enzymes, not only as a tool for the bioremediation of aromatic pollutants,

but also as regio- and stereoselective aromatic-modifying enzymes. With very few exceptions, RO members catalyze the incorporation of both oxygen atoms of molecular dioxygen to tandemly linked carbon atoms in an aromatic ring as two hydroxyl groups in the *cis*-configuration.^{1,2)} This type of dioxygenation is called lateral dioxygenation (LD). For example, LD for anthracene and fluoranthene is shown in Fig. 1A.

Carbazole is an *N*-heterocyclic aromatic compound found in coal tar creosote that is highly recalcitrant, mutagenic, and toxic.³⁾ We have isolated various carbazole degraders, such as *Pseudomonas resinovorans* CA10, *Janthinobacterium* sp. J3, *Novosphingobium* sp. KA1 (formerly *Sphingomonas* sp. KA1), and *Nocardioides aromaticivorans* IC177, and their carbazole degradation pathway and enzymes have been elucidated extensively.⁴⁾ One of the RO members, carbazole 1,9a-

dioxygenase (CARDO), is an initial enzyme in the degradation pathway of carbazole. CARDO attacks at the angular (C-9a) and adjacent (C-1) carbons of carbazole, and the resulting unstable hemiaminal intermediate, 1,9a-dihydroxy-1-hydrocarbazole, is cleaved spontaneously to 2'-aminobiphenyl-2,3-diol (Fig. 1B).^{5,6} This type of reaction is termed angular dioxygenation (AD).^{4,7} CARDO consists of the terminal oxygenase component (CARDO-O, a homotrimer of CarAa proteins) and electron transfer components.^{5,8} In the CARDO systems of *P. resinovorans* CA10 and *Janthinobacterium* sp. J3, electron transfer from NAD(P)H to terminal oxygenase is mediated by ferredoxin (CARDO-F, a monomer of CarAc protein) and ferredoxin reductase (CARDO-R, a monomer of CarAd protein) components.⁸ AD is also involved in the degradation pathways of carbazole-related compounds such as dibenzo-*p*-dioxin, dibenzofuran, and 9-fluorenone,^{4,7} and CARDO can catalyze AD for some of these compounds (Fig. 1B).^{5,6,9} CARDO also catalyzes LD for several polycyclic aromatic hydrocarbons, and monooxygenation for methylene carbon of fluorene and sulfide sulfur of dibenzothiophene (Fig. 1A and C).^{6,9} Although numerous RO members have been isolated and characterized to date, only a limited number of these catalyze AD.

We have determined the crystal structure of CARDO-O from J3 and have performed docking simulation of carbazole to the substrate-binding pocket.¹⁰ In addition, we have succeeded in determining the CARDO-O: CARDO-F:carbazole ternary complex structure, and the docking position of carbazole in the crystal structure.¹¹ The docking structure suggested that the binding of carbazole to CARDO-O was stabilized by hydrogen bonding between the imino nitrogen of carbazole and the carbonyl oxygen of Gly178, and, in this particular case, the C-9a and C-1 carbon atoms of carbazole were situated more closely to the ferrous iron active site. This manner of binding is consistent with the fact that CARDO-O catalyzes AD for carbazole.

Amino acid residues, which constitute the wall of the substrate-binding pocket, are obviously a determinant of carbazole orientation suitable for AD catalysis. We generated 17 CARDO-O mutants that had single amino acid substitutions at the substrate-binding pocket. Based on the oxygenation activities for several substrates, we discuss below the amino acid residues involved in determining the substrate specificity of CARDO-O.

Materials and Methods

Bacterial strains, media, and culture conditions. *Escherichia coli* DH5 α (Toyobo, Tokyo) and JM109¹² were used as host strains for plasmid preparations of pUC119,¹² pT7Blue T-vector (Merck Japan, Tokyo), pBluescript II SK(-) (Stratagene, La Jolla, CA), and their derivatives. *E. coli* JM109 was also used as a host strain in biotransformation experiments. *E. coli* strains

were grown in lysogeny (L)-medium (1% tryptone peptone, 0.5% yeast extract, and 1% NaCl)¹² at 37 °C with reciprocal shaking (300 strokes/min). Ampicillin (Ap; 50 μ g/ml) was added to the selective medium. For plate cultures, the medium was solidified with 1.6% (w/v) agar.

Standard DNA techniques. Restriction endonucleases (Takara Bio, Shiga) and Ligation High (Toyobo) were used according to the manufacturers' instructions. DNA fragments were extracted from agarose gels using an E.Z.N.A. gel extraction kit (Omega Bio-Tek, Doraville, GA). Determination of nucleotide sequences was performed as described previously.¹³ Other DNA manipulations were performed according to standard methods.¹²

Substrate docking simulation to the substrate-binding pocket of CARDO-O. The complex structure of dibenzo-*p*-dioxin and wild-type (WT) CARDO-O of J3 (PDB code, 1WW9) was simulated as described previously.¹⁰ Figures were constructed using PyMOL.¹⁴

Site-directed mutagenesis in the carAa gene. Plasmid pUCARAJ3, which contains the *carAa*, *carAc*, and *carAd* genes from *Janthinobacterium* sp. J3, was constructed as the reference plasmid used for expression of WT CARDO-O. In brief, pBJ3001¹⁵ was digested with *EcoRI*, and the resulting 5.6-kb fragment was inserted into the corresponding restriction sites of modified pUC119, from which the *PstI* site had previously been removed by T4 DNA polymerase treatment followed by self-ligation. The plasmid was then digested with *PstI* and self-ligated to form plasmid pUCARAJ3, which contains the *carAaAcAd* genes and lacks the *carBaBbC* genes.

To replace the target codon of F275, Q282, or F329 in the *carAa* gene with the desired amino acid residues, pTemplateJ, which contains the partial *carAa* gene fragment, was constructed. Initially, a 1.9-kb *BamHI*-*PstI* fragment of pUCARAJ3 containing the entire *carAa* gene and the 5' end of the *carBa* gene was ligated with the corresponding restriction sites of pBluescript II SK(-) to give pJ31BP. The 628-bp *EcoRV* fragment from pJ31BP was inserted into the same site of pBluescript II SK(-) to create plasmid pTemplateJ. For replacement of the I262 codon, pTemplateJ-II was constructed as follows: pJ31BPC was formed by ligation of the 1.2-kb *ClaI* fragment of pJ31BP with *ClaI*-treated pBluescript II SK(-). Plasmid pJ31BPC was then digested with *ApaI* and self-ligated, and the resulting plasmid was designated pTemplateJ-II.

Site-directed mutagenesis was performed using the QuickChange XL Site-Directed Mutagenesis Kit (Stratagene) according to the manufacturer's instructions. A template plasmid, *viz.*, pTemplateJ or pTemplateJ-II, and two complementary oligonucleotide primers containing the desired mutation were used. Detailed information on the primers used is available

upon request. Following mutagenesis, preferred nucleotide replacements were confirmed by sequencing, and the resulting plasmids were labeled as shown in Table 1 (pTemplateJ-F275A or pTemplateJ-II-I262A). According to the reverse scheme from pUCARAJ3 to pTemplateJ/J-II, we constructed pUCARAJ3 derivatives, which had the desired replacements in the *carAa* gene, to express the site-directed mutations of CARDO-O (Table 1).

Biotransformations. *E. coli* JM109 harboring pUCARAJ3 or its derivatives was precultured in 5 ml of L-medium supplemented with Ap at 37 °C for 12 h, followed by 1-ml aliquot transfer of the resulting culture to 250 ml of L-medium. After incubation at 25 °C for 5 h, isopropyl- β -D-thiogalactopyranoside was added to a final concentration of 0.1 mM. After an additional 15 h of incubation, the cells were harvested by centrifugation, washed twice with MM3 (2.2 g/l Na₂HPO₄, 0.8 g/l KH₂PO₄, 500 mg/l MgSO₄·7H₂O, 10 mg/l FeSO₄·7H₂O, 10 mg/l CaCl₂·2H₂O, 50 mg/l yeast extract), and resuspended in MM3 adjusted to an OD₆₀₀ of 20. As substrates, we used carbazole, dibenzo-*p*-dioxin, anthracene, fluorene, fluoranthene, and dibenzothiophene. Each substrate, except for anthracene, was dissolved in dimethylsulfoxide (10 mg/ml); 50 μ l of the resulting solution was added to 5 ml of cell suspension. Anthracene was dissolved in *N,N*-dimethylformamide (10 mg/ml) and similarly added to the cell suspension. The reaction mixtures were incubated on a reciprocal shaker (300 strokes/min) at 30 °C for 18 h.

The reaction mixtures were extracted with ethyl acetate, and the ethyl acetate layer was dried over anhydrous Na₂SO₄. A portion of each extract was directly analyzed by gas chromatography-mass spectrometry (GC-MS) after trimethylsilylation with *N*-methyl-*N*-trimethylsilyltrifluoroacetamide (MSTFA) at 70 °C for 20 min, except for the quantification of dibenzothiophene and its oxygenation products. GC-MS was performed as described previously.⁶⁾ The products were identified by comparison of their mass spectra with data from previous reports.^{6,9,16,17)} To quantify the products formed and the remaining substrate, we compared the peak areas for the total ion current of the respective compounds extracted from the reaction mixtures containing *E. coli* cells that harbored pUCARAJ3 derivatives. The product formation rate was calculated from the peak area of the product divided by the sum of the peak areas of the product formed and the remaining substrate.

Quantification of the remaining dibenzothiophene and its oxygenation products was done by monitoring their respective A_{220s} using high-performance liquid chromatography (HPLC). HPLC was done using a Senshu-Pak ODS 1251-D column (4.6 by 250 mm; Senshu Scientific, Tokyo). The solvent flow rate was 0.8 ml/min, and the column was maintained at 30 °C. A portion of the ethyl acetate extract from the reaction mixture was dried

under a nitrogen stream and redissolved into 100 μ l of methanol solution (40% methanol by volume of water). The resulting sample was injected into a column equilibrated with methanol/water (4:6 v/v) and eluted with an increasing gradient of methanol/water. The methanol in the mobile phase was increased to 60% for 25 min, followed by an increase to 100% for 20 min.

Identification of products formed by CARDO-O mutants. In carbazole biotransformation experiments using several CARDO-O mutants, we detected monohydroxycarbazole having an R_f of 0.61 by analytical thin-layer chromatography (TLC) with a solvent system of hexane-ethyl acetate-acetic acid (6:4:0.5 by volume). To purify this compound, preparative TLC was performed as follows: TLC was developed on a precoated silica gel plate (1 mm in thickness, 20 × 20 cm, Silica gel 60 F₂₅₄, Merck Japan) with the same solvent system as analytical TLC. The desired band was scraped off and eluted with H₂O-saturated ethyl acetate. The resulting elute was dried with Na₂SO₄ before evaporation and used in nuclear magnetic resonance (NMR) spectrometry. The ¹H and ¹³C NMR spectra of the compound were recorded using an ECA-600 spectrometer (JEOL, Tokyo) operated at 600 and 150 MHz respectively, with TMS as an internal standard. Two-dimensional NMR experiments for the determination of direct ¹H-¹³C connectivity (HSQC), long-range (two- and three-bond) ¹H-¹³C connectivity (HMBC), measurements of nuclear Overhauser enhancement spectroscopy (NOESY), and ¹H-¹H shift-correlated spectroscopy (¹H-¹H DQF-COSY) were done under the above conditions.

We observed a marked increase in the putative monohydroxyl derivative of fluorene on GC-MS analysis of the biotransformation product by the F275W mutant enzyme. A preparative TLC with a solvent system of hexane-ethyl acetate (2:1, by volume) gave R_f = 0.6 for this product. The desired product was scraped off, purified, and identified by NMR, as described above.

Western blots. Crude cell extract of *E. coli* in which the expression of CARDO-O mutant was induced as described above was prepared by sonication and subsequent centrifugation. Protein concentrations were estimated using a protein assay kit (Bio-Rad Laboratories, Tokyo) with BSA as standard by the method described by Bradford.¹⁸⁾ A 100 to 1,000- μ g aliquot of denatured crude cell extract was subjected to SDS-12% polyacrylamide gel electrophoresis (SDS-PAGE) and electrophoretically transferred onto PVDF membranes using the iBlot Gel Transfer System (Invitrogen, Tokyo). The CarAa protein (CARDO-O subunit) was detected immunologically using a rabbit polyclonal antibody as the primary antibody and horseradish peroxidase-linked anti-rabbit Ig (GE Healthcare Bio-Sciences, Tokyo) as the secondary antibody. A CarAa-specific polyclonal antibody was prepared by Sigma

Table 1. Plasmids Used in This Study

Plasmid	Relevant characteristics	Source or reference
pBJ3001	Ap ^r , pBluescript II KS(−) with 5.6-kb <i>EcoRI</i> fragment from J3, <i>carAaBaBbCAcAd</i>	15
pBluescript II SK(−)	Ap ^r , <i>lacZ</i> , pMB9 replicon	Stratagene
pJ31BP	Ap ^r , pBluescript II SK(−) with 1.9-kb <i>BamHI-PstI</i> fragment of J3, <i>carAa</i>	This study
pJ31BP-F275A	pJ31BP derivative, Triplet codon for F275 is replaced with GCG	This study
pJ31BP-F275I	pJ31BP derivative, Triplet codon for F275 is replaced with ATT	This study
pJ31BP-F275L	pJ31BP derivative, Triplet codon for F275 is replaced with CTG	This study
pJ31BP-F275V	pJ31BP derivative, Triplet codon for F275 is replaced with GTG	This study
pJ31BP-F275W	pJ31BP derivative, Triplet codon for F275 is replaced with TGG	This study
pJ31BP-F329A	pJ31BP derivative, Triplet codon for F329 is replaced with GCG	This study
pJ31BP-F329I	pJ31BP derivative, Triplet codon for F329 is replaced with ATT	This study
pJ31BP-F329L	pJ31BP derivative, Triplet codon for F329 is replaced with CTG	This study
pJ31BP-F329V	pJ31BP derivative, Triplet codon for F329 is replaced with GTG	This study
pJ31BP-F329W	pJ31BP derivative, Triplet codon for F329 is replaced with TGG	This study
pJ31BP-I262A	pJ31BP derivative, Triplet codon for I262 is replaced with GCG	This study
pJ31BP-I262L	pJ31BP derivative, Triplet codon for I262 is replaced with CTG	This study
pJ31BP-I262V	pJ31BP derivative, Triplet codon for I262 is replaced with GTG	This study
pJ31BP-I262W	pJ31BP derivative, Triplet codon for I262 is replaced with TGG	This study
pJ31BP-Q282N	pJ31BP derivative, Triplet codon for Q282 is replaced with AAT	This study
pJ31BP-Q282S	pJ31BP derivative, Triplet codon for Q282 is replaced with TCG	This study
pJ31BP-Q282Y	pJ31BP derivative, Triplet codon for Q282 is replaced with TAC	This study
pJ31BPC	Ap ^r , pBluescript II SK(−) containing 1.2-kb <i>Clal</i> insert of pJ31BP	This study
pJ31BPC-I262A	pJ31BPC derivative, Triplet codon for I262 is replaced with GCG	This study
pJ31BPC-I262L	pJ31BPC derivative, Triplet codon for I262 is replaced with CTG	This study
pJ31BPC-I262V	pJ31BPC derivative, Triplet codon for I262 is replaced with GTG	This study
pJ31BPC-I262W	pJ31BPC derivative, Triplet codon for I262 is replaced with TGG	This study
pT7Blue T-vector	Ap ^r , <i>lacZ</i> , f1 ori, T7 promoter, pUC/M13 priming sites	Merck Japan
pTemplateJ	Ap ^r , pBluescript II SK(−) with 628-bp <i>EcoRV</i> fragment from pJ31BP	This study
pTemplateJ-F275A	pTemplateJ derivative, Triplet codon for F275 is replaced with GCG	This study
pTemplateJ-F275I	pTemplateJ derivative, Triplet codon for F275 is replaced with ATT	This study
pTemplateJ-F275L	pTemplateJ derivative, Triplet codon for F275 is replaced with CTG	This study
pTemplateJ-F275V	pTemplateJ derivative, Triplet codon for F275 is replaced with GTG	This study
pTemplateJ-F275W	pTemplateJ derivative, Triplet codon for F275 is replaced with TGG	This study
pTemplateJ-F329A	pTemplateJ derivative, Triplet codon for F329 is replaced with GCG	This study
pTemplateJ-F329I	pTemplateJ derivative, Triplet codon for F329 is replaced with ATT	This study
pTemplateJ-F329L	pTemplateJ derivative, Triplet codon for F329 is replaced with CTG	This study
pTemplateJ-F329V	pTemplateJ derivative, Triplet codon for F329 is replaced with GTG	This study
pTemplateJ-F329W	pTemplateJ derivative, Triplet codon for F329 is replaced with TGG	This study
pTemplateJ-Q282N	pTemplateJ derivative, Triplet codon for Q282 is replaced with AAT	This study
pTemplateJ-Q282S	pTemplateJ derivative, Triplet codon for Q282 is replaced with TCG	This study
pTemplateJ-Q282Y	pTemplateJ derivative, Triplet codon for Q282 is replaced with TAC	This study
pTemplateJ-II	Ap ^r , pBluescript II SK(−) containing 833-bp <i>Clal-ApaI</i> insert of pJ31BPC	This study
pTemplateJ-II-I262A	pTemplateJ-II derivative, Triplet codon for I262 is replaced with GCG	This study
pTemplateJ-II-I262L	pTemplateJ-II derivative, Triplet codon for I262 is replaced with CTG	This study
pTemplateJ-II-I262V	pTemplateJ-II derivative, Triplet codon for I262 is replaced with GTG	This study
pTemplateJ-II-I262W	pTemplateJ-II derivative, Triplet codon for I262 is replaced with TGG	This study
pUC119	Ap ^r , <i>lacZ</i> , f1 ori, M13 priming sites	12
pUCARA	Ap ^r , modified pUC119 (lacking <i>PstI</i> site in multi-cloning site) with 5.6-kb <i>EcoRI</i> insert of pUCA1 with the deletion of 1.3-kb <i>PstI-BglII</i> fragment, <i>carAaAaAcAd</i>	5
pUCARAJ3	Ap ^r , modified pUC119 (lacking <i>PstI</i> site in multi-cloning site) with 3.8-kb <i>EcoRI</i> fragment from J3 in which 1.7-kb <i>PstI</i> fragment containing <i>carBaBbC</i> region was deleted, <i>carAaAcAd</i>	This study
pUCARAJ3-F275A	pUCARAJ3 derivative, expressing F275A CARDO-O mutant	This study
pUCARAJ3-F275I	pUCARAJ3 derivative, expressing F275I CARDO-O mutant	This study
pUCARAJ3-F275L	pUCARAJ3 derivative, expressing F275L CARDO-O mutant	This study
pUCARAJ3-F275V	pUCARAJ3 derivative, expressing F275V CARDO-O mutant	This study
pUCARAJ3-F275W	pUCARAJ3 derivative, expressing F275W CARDO-O mutant	This study
pUCARAJ3-F329A	pUCARAJ3 derivative, expressing F329A CARDO-O mutant	This study
pUCARAJ3-F329I	pUCARAJ3 derivative, expressing F329I CARDO-O mutant	This study
pUCARAJ3-F329L	pUCARAJ3 derivative, expressing F329L CARDO-O mutant	This study
pUCARAJ3-F329V	pUCARAJ3 derivative, expressing F329V CARDO-O mutant	This study
pUCARAJ3-F329W	pUCARAJ3 derivative, expressing F329W CARDO-O mutant	This study
pUCARAJ3-I262A	pUCARAJ3 derivative, expressing I262A CARDO-O mutant	This study
pUCARAJ3-I262L	pUCARAJ3 derivative, expressing I262L CARDO-O mutant	This study
pUCARAJ3-I262V	pUCARAJ3 derivative, expressing I262V CARDO-O mutant	This study
pUCARAJ3-I262W	pUCARAJ3 derivative, expressing I262W CARDO-O mutant	This study
pUCARAJ3-Q282N	pUCARAJ3 derivative, expressing Q282N CARDO-O mutant	This study
pUCARAJ3-Q282S	pUCARAJ3 derivative, expressing Q282S CARDO-O mutant	This study
pUCARAJ3-Q282Y	pUCARAJ3 derivative, expressing Q282Y CARDO-O mutant	This study

Genosys (Ishikari, Japan) using the native (non-His-tagged) form of the CarAa protein from CA10 that was overexpressed by *E. coli* cells and purified as described previously.⁸⁾ Western blots were performed using Immobilon Western (Nihon Millipore, Tokyo) according to the manufacturer's instructions. CarAa protein signals were visualized using Luminescent Image Analyzer LAS-1000 plus (Fuji Photo Film, Tokyo).

Results

Preparation of CARDO-O mutants by site-directed mutagenesis

To identify the possible amino acid residues affecting the binding of substrate to CARDO-O, we first performed a docking simulation of dibenzo-*p*-dioxin, for which CARDO catalyzed AD. The computer-predicted docking positions of dibenzo-*p*-dioxin rarely differed (Fig. 2A), and the root-mean-square difference of non-hydrogen atoms of the 10 members from its cluster center was less than 1.08 Å. This manner of binding for dibenzo-*p*-dioxin is in accord with the catalysis of AD (*cis*-1,10a-dihydroxylation) by CARDO-O, and was well superposed on the positions of the carbazole binding in the CARDO-O:CARDO-F:carbazole ternary complex structure¹¹⁾ (Fig. 2B).

Except for the ligands for ferrous iron active site, there are six amino acids within 3.6 Å distance from any atoms of carbazole molecule. Among them, I184 is the amino acid neighboring to the active site ligand, H183, and N^{δ2} of N330 forms hydrogen bond with O^{δ2} of D333, the ligand of the ferrous ion active site. In this situation, their replacements were expected to affect the active site geometry and to affect the CARDO-O catalytic activity itself. Based on this consideration, we selected amino acid residues I262, F275, Q282, and F329, which can affect the catalysis of AD by CARDO-O. Accordingly, we generated site-directed mutants by replacing a single amino acid residue with similar amino acid residues of different size in the side chain in each one of the above four residues (*viz.*, for Ile: Ala, Val, Leu, and Trp; for Phe: Ala, Val, Leu, Ile, and Trp; and for Gln: Ser, Tyr, and Asn).

Production of CARDO-O mutants in E. coli cells

Using the *E. coli* JM109 expressing the CARDO-O mutant in conjunction with CARDO-F and CARDO-R from *Janthinobacterium* sp. J3, crude cell extracts were prepared and subjected to Western blotting using CarAa-specific antibody. The WT and all of the CARDO-O mutants produced a full-length soluble protein with a small variation in the amount of each mutant protein obtained (Fig. 3).

Oxygenating activity of the site-directed mutants of CARDO-O

We carried out biotransformation experiments with carbazole, dibenzo-*p*-dioxin, anthracene, fluorene, fluo-

ranthene, and dibenzothiophene. The quantification of the products formed by all CARDO-O mutants is summarized in Tables 2–4. Compared to our previous results using the WT CARDO system from *P. resinovorans* CA10,^{6,9)} we did not detect any significant difference in the substrate preference or product formation capability of the WT CARDO system from J3.

*Dibenzo-*p*-dioxin and anthracene*

In biotransformation experiments using several mutant and WT enzymes, we detected production of 2,2',3'-trihydroxydiphenyl ether formed by AD with dibenzo-*p*-dioxin, followed by spontaneous central ring-cleavage reactions (Table 2). No other products, such as *cis*-dihydrodiols of dibenzo-*p*-dioxin or their putative dehydration product and monohydroxydibenzo-*p*-dioxin, were detected.

In comparison with previous data from GC-MS, anthracene was converted to anthracene-1,2-dihydrodiol, a major product of CARDO from CA10,⁶⁾ by WT CARDO from J3 and several of its mutants. In addition, another anthracene *cis*-dihydrodiol-like compound was detected by GC-MS [356 (M⁺, 43), 341 (25), 266 (40), 178 (25), 73 (100)] and was assumed to be 2,3-dihydrodiol, because anthracene has two tandemly linked vicinal carbon atom pairs for which LD is possibly catalyzed (Table 2).

The oxygenation capabilities of the CARDO-O mutants observed for dibenzo-*p*-dioxin had a tendency similar to those for anthracene, although these two substrates were catalyzed primarily by AD and LD respectively. Generally, mutants having the replacement at F275 or F329 had no or dramatically reduced oxygenation activity for these substrates, except for the F275W mutant. In contrast, the I262L, I262V, F275W, and Q282Y mutants showed relatively high oxygenation activity for these substrates among the I262- and Q282-substituents, although the oxygenation activity of I262A, I262W, and Q282N decreased markedly. It is noteworthy that production of the putative 2,3-dihydrodiol of anthracene, a minor product of the WT enzyme, was highly increased in F275W as compared to the production of anthracene-1,2-dihydrodiol.

Carbazole

Although F329-replaced mutants showed only negligible oxygenase activity, most mutant enzymes produced 2'-aminobiphenyl-2,3-diol, which is generated by AD followed by spontaneous rearomatization and hetero-ring cleavage, as the main product from carbazole (Table 2). In addition to the AD product, I262A, I262L, I262V, F275W, and Q282-replaced mutants yielded another product from carbazole. In the case of the I262V and Q282Y mutants, the amount of new product detected equal to or was of higher than that of 2'-aminobiphenyl-2,3-diol. GC-MS showed that the TMS derivative of the new product had the presumed molecular ion peak at *m/z* 255, implying that this

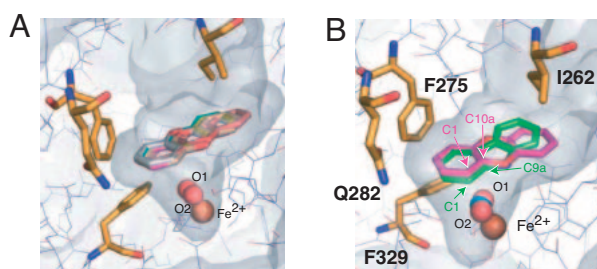


Fig. 2. Computer-Predicted Docking Structures of Dibenzo-*p*-dioxin in the CARDO-O Active Site (A) and a Comparison with the Carbazole-Binding Position in the CARDO-O: CARDO-F: Carbazole Ternary Complex Structure (B).¹¹

Ten representative binding conformations of dibenzo-*p*-dioxin to dioxygen-bound CARDO-O are shown in panel A. In panel B, the cluster center of the 10 dibenzo-*p*-dioxin-docking structures and carbazole-docking crystal structure are colored magenta and green respectively. In both panels, the catalytic mononuclear irons, the modeled dioxygen bound to the active site, and the ligand water in the crystal structure are shown in the CPK model, and are colored brown, red, and marine blue respectively. Ile262, Phe275, Gln282, and Phe329 residues, which were replaced with similar amino acid residues in this study, are shown in the wire-frame model, and are colored gold.

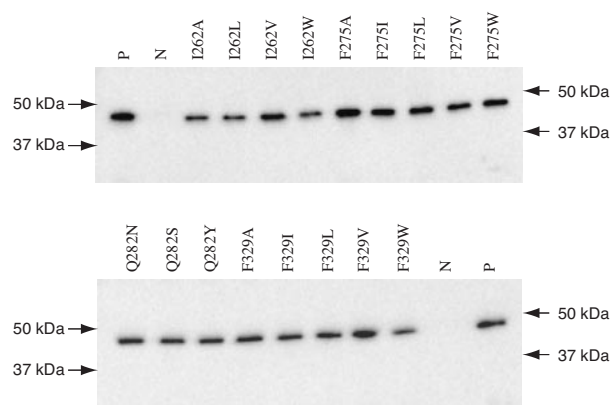


Fig. 3. Western Blots of *E. coli* Cell Lysates Expressing CARDO-O Mutants Using the CARDO-O-Specific Antibody.

A rabbit polyclonal antibody specific for the CarAa protein, which is a subunit of CARDO-O, was used, as described in "Materials and Methods." A 0.15- μ g aliquot of soluble proteins isolated from *E. coli* cells was loaded for SDS-PAGE. "P" and "N" mean positive control (soluble protein of *E. coli* JM109(pUCARAJ3)) and negative control (soluble protein of *E. coli* JM109(pUC119)) respectively.

product was monohydroxycarbazole [255 (M^+ , 100), 239 (52), 224 (46), 209 (20), 73 (33)]. Its fragmentation pattern was similar to those of the TMS derivatives of the authentic 2-hydroxy- and 4-hydroxycarbazole, but its GC retention time was different from those of these TMS derivatives (data not shown). The ^1H NMR spectra of the product in CDCl_3 showed chemical shifts (δ ppm) with chemical shift multiplicities (d, doublet; t, triplet, coupling constants, J in Hz, in parentheses), as follows: 6.83 (d, $J = 7.78$ Hz, H-2), 7.06 (t, $J = 7.78$ Hz, H-3), 7.21 (t, $J = 7.01$ Hz, H-6), 7.40 (t, $J = 7.02$ Hz, H-7),

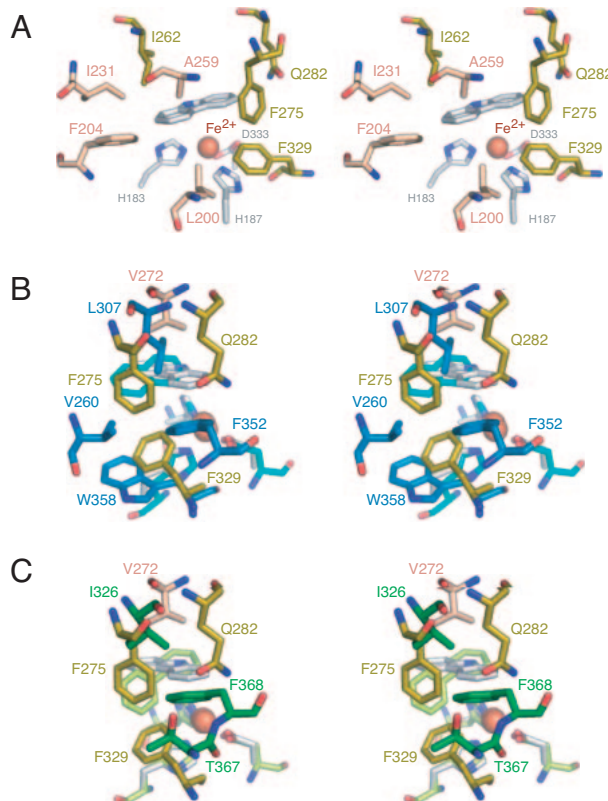


Fig. 4. Stereoview of the Amino Acid Residues Possibly Affecting the Substrate Specificity of CARDO from *Janthinobacterium* sp. J3 (A), and a Comparison with Those in NDO-O from *Pseudomonas* sp. NCIB9816-4 (B) and BDO-O from *Rhodococcus jostii* RHA1 (C).

In panel A, intended amino acid residues around the ferrous iron active sites, including ligands (gray), target amino acids for site-directed mutagenesis (gold), and other possible determinants of substrate specificity (wheat) are shown in the wire-frame model. Catalytic mononuclear irons are shown as spheres. Carbazole is also shown in the wire-frame model, colored gray. In panels B and C, ferrous iron, and CARDO-O amino acid residues are shown as in panel A. The ligands of the ferrous iron active site, substrate, and amino acid residues affecting substrate specificities of NDO-O (in panel B) and BDO-O (in panel C) are colored blue and green respectively.

7.45 (d, $J = 8.24$ Hz, H-8), 7.65 (d, $J = 7.93$ Hz, H-4), 8.04 (d, $J = 7.78$ Hz, H-5). In addition, the ^{13}C NMR for this compound showed signals at δ 110.70 (C-2), 111.00 (C-8), 112.95 (C-4), 119.42 (C-6), 119.80 (C-3), 120.64 (C-5), 123.73 (C), 125.32 (C), 125.91 (CH), 129.18 (C), 139.51 (CH), and 141.51 (C-1). Based on the results of the ^1H - ^1H COSY spectra (data not shown), we identified the compound as 1-hydroxycarbazole. Therefore, the CARDO-O mutants mentioned above acquired the ability to convert carbazole to 1-hydroxycarbazole, which was assumed to be created by the spontaneous dehydration of primary *cis*-dihydroxylation products.

A comparison of oxygenation activity for dibenzo-*p*-dioxin and carbazole showed that the F275V, Q282N, and Q282S mutants retained relatively high AD activity for carbazole, but showed only low or negligible AD activity for dibenzo-*p*-dioxin, although the WT enzyme catalyzes AD for these two substrates as a primary reaction.

Table 2. Products Formed from Carbazole, Dibenzo-*p*-dioxin, and Anthracene by CARDO-O Mutants^a

	From carbazole		From dibenzo- <i>p</i> -dioxin	From anthracene	
	2'-Aminobiphenyl-2,3-diol ^b	1-Hydroxy-carbazole ^b	2,2',3-Trihydroxy-diphenyl ether ^b	Anthracene-1,2-dihydrodiol ^b	Putative anthracene 2,3-dihydrodiol ^b
Wild-type	99.1 (0.07)	Trace	88.7 (1.56)	20.8 (1.82)	6.17 (0.40)
I262A	32.0 (1.26)	1.67 (1.74)	20.0 (7.15)	1.06 (0.06)	Trace
I262L	95.3 (0.24)	4.71 (0.24)	90.5 (1.32)	83.7 (5.22)	1.84 (0.24)
I262V	26.3 (9.27)	16.2 (1.26)	37.5 (1.80)	8.25 (0.46)	Trace
I262W	31.5 (2.18)	N.D.	18.8 (5.60)	1.69 (1.49)	N.D.
F275A	24.4 (0.78)	N.D.	9.63 (5.60)	3.24 (1.81)	N.D.
F275I	45.3 (2.62)	N.D.	N.D.	N.D.	N.D.
F275L	3.14 (0.95)	N.D.	Trace	N.D.	N.D.
F275V	18.1 (7.22)	Trace	1.04 (0.31)	N.D.	N.D.
F275W	91.8 (1.62)	8.15 (1.63)	97.8 (0.27)	18.1 (0.10)	22.7 (1.65)
Q282N	63.9 (1.93)	3.90 (0.95)	2.38 (0.68)	N.D.	N.D.
Q282S	33.8 (5.00)	2.63 (2.90)	12.9 (9.60)	2.34 (2.21)	2.21 (0.10)
Q282Y	39.3 (1.91)	46.8 (5.97)	43.8 (2.77)	11.1 (9.73)	1.11 (0.98)
F329A	Trace	Trace	N.D.	N.D.	N.D.
F329I	Trace	Trace	Trace	N.D.	N.D.
F329L	Trace	Trace	Trace	N.D.	N.D.
F329V	Trace	Trace	N.D.	N.D.	N.D.
F329W	Trace	N.D.	N.D.	N.D.	N.D.

^a“Trace” means that the product formation estimated was less than 1%. “N.D.” means that product formation was not detected. Values in parentheses represent standard deviations calculated from at least three assays.

^bTo quantify the products formed in GC-MS analyses, we compared the peak areas for the total ion current of the respective compounds extracted from the reaction mixtures containing *E. coli* cells that harbored pUCARAJ3 derivatives. The product formation rate was calculated from the peak area of the product divided by the sum of the peak areas of the product formed and the remaining substrate.

Table 3. Products Formed from Fluorene and Fluoranthene by CARDO-O Mutants^a

	From fluorene		From fluoranthene		
	9-Hydroxyfluorene ^b	4-Hydroxyfluorene ^b	7-Hydroxy-fluoranthene ^b	<i>cis</i> -2,3-Dihydroxy-2,3-dihydrofluoranthene ^b	Putative <i>cis</i> -dihydrodiol of fluoranthene ^b
Wild-type	5.86 (0.18)	3.03 (0.70)	Trace	Trace	N.D.
I262A	Trace	N.D.	N.D.	N.D.	N.D.
I262L	6.80 (0.16)	Trace	Trace	Trace	N.D.
I262V	Trace	Trace	N.D.	Trace	N.D.
I262W	1.01 (0.02)	N.D.	N.D.	N.D.	N.D.
F275A	4.12 (0.98)	N.D.	Trace	Trace	9.72 (1.60)
F275I	1.24 (0.06)	N.D.	N.D.	N.D.	N.D.
F275L	Trace	N.D.	N.D.	N.D.	N.D.
F275V	1.07 (0.30)	N.D.	N.D.	N.D.	N.D.
F275W	3.90 (1.81)	22.6 (1.47)	Trace	Trace	N.D.
Q282N	Trace	Trace	N.D.	Trace	N.D.
Q282S	Trace	N.D.	N.D.	Trace	N.D.
Q282Y	1.19 (0.11)	Trace	N.D.	Trace	N.D.
F329A	2.67 (0.02)	N.D.	N.D.	N.D.	N.D.
F329I	2.23 (1.20)	Trace	N.D.	N.D.	N.D.
F329L	2.47 (1.26)	N.D.	N.D.	N.D.	N.D.
F329V	2.95 (0.41)	N.D.	N.D.	N.D.	N.D.
F329W	2.91 (1.46)	N.D.	N.D.	N.D.	N.D.

^a“Trace” means that the product formation estimated was less than 1%. “N.D.” means that product formation was not detected. Values in parentheses represent standard deviations calculated from at least three assays.

^bTo quantify the products formed in GC-MS analyses, we compared the peak areas for the total ion current of the respective compounds extracted from the reaction mixtures containing *E. coli* cells that harbored pUCARAJ3 derivatives. The product formation rate was calculated from the peak area of the product divided by the sum of the peak areas of the product formed and the remaining substrate.

Fluorene

The oxygenation activity of the WT and mutant CARDO-O enzymes for fluorene were noticeably lower than those for carbazole (Table 3), but only F275W

showed relatively high oxygenating activity for fluorene. Although F275W catalyzed 9-hydroxylation of fluorene at an efficiency as low as that of the WT, the yield of another product was increased to approximately 22.6%.

Table 4. Products Formed from Dibenzothiophene by Wild-Type and CARDO Mutants^a

	From dibenzothiophene	
	Dibenzothiophene 5-oxide ^b	Putative monohydroxy-dibenzothiophenes ^{b,c}
Wild-type	70.8 (1.58)	10.7 (2.02)
I262A	47.2 (3.77)	45.3 (8.16)
I262L	89.2 (1.20)	7.70 (1.23)
I262V	84.6 (2.08)	5.33 (2.08)
I262W	21.3 (3.52)	41.9 (6.54)
F275A	30.6 (8.15)	21.6 (7.64)
F275I	N.D.	N.D.
F275L	N.D.	N.D.
F275V	N.D.	N.D.
F275W	90.2 (2.15)	7.38 (1.61)
Q282N	12.2 (3.23)	7.12 (2.96)
Q282S	65.2 (6.84)	8.33 (1.53)
Q282Y	53.0 (2.33)	6.34 (2.72)
F329A	N.D.	N.D.
F329I	N.D.	N.D.
F329L	N.D.	N.D.
F329V	N.D.	N.D.
F329W	N.D.	N.D.

^a“N.D.” means that product formation was not detected.

^bTo quantify the products formed, we compared the peak areas in HPLC analyses for the respective A₂₂₀s of the compounds extracted from reaction mixtures containing *E. coli* cells that harbored pUCARAJ3 derivatives. The product formation rate was calculated from the peak area of the product divided by the sum of the peak areas of the product formed and the remaining substrate.

^cAt least three monohydroxyl derivatives were included in the products.

This second product was also produced by the WT, but the production yield was markedly low (approximately 3%). GC-MS showed that the TMS derivative of the unidentified product had the assumed molecular ion peak at m/z 254, implying that this product was monohydroxyfluorene [254 (M^+ , 90), 239 (41), 223 (100), 165 (12), 152 (10)]. Although its fragmentation pattern was similar to that of the TMS derivatives of authentic 2-hydroxyfluorene, its GC retention time was different. The ¹H NMR spectra of the product in CDCl₃ showed chemical shifts (δ ppm, chemical shifts multiplicities and coupling constants in parentheses) as follows: 6.73 (d, $J = 6.0$ Hz, H-3), 7.14 (d, $J = 7.0$ Hz, H-1), 7.15 (t, $J = 6.8$ Hz, H-2), 7.27 (t, $J = 7.3$ Hz, H-7), 7.37 (t, $J = 7.5$ Hz, H-6), 7.51 (d, $J = 7.5$ Hz, H-8), 8.10 (d, $J = 7.5$ Hz, H-5). In addition, the ¹³C NMR for this compound showed signals at δ 113.67 (C-3), 117.61 (C-1), 123.45 (C-5), 124.44 (C-8), 125.92 (C-7), 126.77 (C-6), 127.49 (C-2), 128.60 (CH), 140.62 (C), 142.49 (C), 145.86 (CH), and 151.51 (C-4). Based on the results of the COSY spectra, the NOESY spectra, and HMBC (data not shown), we identified the compound as 4-hydroxyfluorene.

Fluoranthene

Although conversion of fluoranthene to 7-hydroxyfluoranthene and/or *cis*-2,3-dihydroxy-2,3-dihydrofluoranthene was detected in the WT and some mutant

CARDO-O enzymes, most mutant enzymes lost all fluoranthene-oxygenating activity (Table 3), but the F275A mutant yielded a new and noteworthy product. GC-MS of the TMS derivative of this new product provided a fragmentation pattern 380 (M^+ , 78), 259 (10), 202 (28), 147 (26), 73 (100) and the putative molecular ion peak, suggesting that the new product was *cis*-dihydrodiol of fluoranthene. However, definite identification of this product by NMR could not be made due to a low conversion ratio.

Dibenzothiophene

In a biotransformation experiment using the WT enzyme, we detected dibenzothiophene-5-oxide as the major product from dibenzothiophene, similarly to previous results (Table 4).^{6,9} The overall tendency in oxygenation capability for dibenzothiophene observed in mutants was roughly similar to those for other substrates. A marked decrease or complete loss of oxygenating activity was detected in some of the F275-replaced mutants and in all of the F329-replaced mutants. Active mutants could be divided into two groups: mutants exhibiting activity similar to WT activity (I262L, I262V, F275W, Q282S, and Q282Y) and mutants producing rather large amounts of other products from dibenzothiophene (I262A, I262W, and F275A). The new products displayed UV spectrum maxima at 256 and 285 nm. GC-MS of the HPLC-fractionated new products (HPLC retention time, 40.5 min) suggested that this fraction contained three products that had similar MS fragmentation patterns, as follows: 272 (M^+ , 73), 257 (100), 197 (12), 139 (16), 73 (21); 272 (M^+ , 100), 257 (89), 184 (17), 139 (18), 73 (17); 272 (M^+ , 63), 257 (65), 117 (56), 71 (68), 57 (100). In comparison with the previous results using WT CARDO-O from CA10,^{6,9} these products are proposed to be monohydroxy derivatives of dibenzothiophene.

Discussion

To understand the molecular mechanism governing the substrate specificity of CARDO, we generated CARDO-O mutants that had different substrate specificities from WT CARDO-O. Detailed studies of the substrate specificity of CARDO were performed using CARDO from *P. resinovorans* CA10.^{6,9} Because the first trial in determining the crystal structure of CARDO-O from CA10 failed, we used CARDO-O from *Janthinobacterium* sp. J3 in X-ray crystallography, and succeeded in obtaining the three-dimensional structures of CARDO-O and its ternary complex form with CARDO-F and carbazole.^{10,11} The structure of the substrate-binding pocket and the manner of carbazole binding around the ferrous iron active site provided us with information on the amino acid residues constituting the substrate-interacting surface around the ferrous iron active site and an important cue to the targets for amino acid substitution to improve or modify the activity of

this novel enzyme (Fig. 2). Based on this information, we created site-directed mutants at the F275, Q282, and F329 residues and the I262 residue of CARDO-O from J3 and determined their oxygenation activities for several substrates. The former three amino acid residues are located near the bottom of the substrate-binding pocket and are close to the aromatic ring to be oxidized. The latter amino acid residue is located near the entrance of the substrate-binding pocket and is close to another aromatic ring (Figs. 2 and 4). All mutants expressed CARDO-O at similar efficiency as the WT CARDO-O, implying that most substitutions did not affect the folding or the stability of the CARDO-O protein. Accordingly, the product-forming activities detected in the biotransformation experiments indicated the substrate specificities of the mutant enzymes.

Based on our results using the WT enzyme, we did not detect significant differences between the substrate specificities of CARDO-O from CA10^{6,9)} and that from J3. This result may be because the two CARDO-O molecules of different origin have only three amino acid substitutions in the regions farthest from the substrate-binding pocket and ferredoxin-binding surface (data not shown).

The crystal structure of the carbazole-bound form of CARDO-O clearly suggests that two benzene moieties of carbazole interact with the hydrophobic wall in the substrate-binding pocket. In addition, the binding of carbazole is stabilized in a single orientation by hydrogen-bonding between imino nitrogen and carbonyl oxygen of G178.¹¹⁾ Unlike carbazole, dibenzo-*p*-dioxin and anthracene have no functional group affecting their orientation in the substrate-binding pocket, and the binding of these substrates appeared to be stabilized only by hydrophobic interactions between the substrate and the wall of the substrate-binding pocket. Considering that these two substrates have similar three-ring fused planar structures, it is reasonable to suggest that they bind in a similar manner around the ferrous iron active site of the WT CARDO-O and most CARDO-O mutants. This coincides with the fact that the oxygenation capability of the mutant CARDO-Os for these two substrates was essentially unaffected.

Among the amino acid residues in which replacement was done, the phenyl moiety of F275 appears to be directly involved in the stacking interaction with the benzene ring of carbazole, which is hydroxylated. In fact, the F275 replacement with amino acid residues that have aliphatic side chains dramatically reduced the oxygenation activity for the substrates tested (Tables 2–4). The above-mentioned role of F275 in substrate binding appears to coincide with our results for the fluorene biotransformation experiments. When fluorene was added as a substrate for WT CARDO-O and its mutants, we detected only weak oxygenation activity (Table 3), but the F275W mutant showed elevated oxygenation activity, and 4-hydroxyfluorene was detected as a major product. These results imply that fluorene does not bind

tightly around the ferrous iron active site in the WT and in most of the mutant CARDO-Os. The indole moiety of W275 in the F275W mutant formed a strengthened stacking interaction with the benzene moiety of the substrate. The bulky indole moiety might change the orientation of the fluorene bound around the ferrous iron active site, resulting in the formation of 4-hydroxyfluorene as a major product. Another interesting CARDO-O mutant is F275A, which showed unique oxygenation activity for fluoranthene (Table 3). Although the oxygenation activity of the WT and mutants of CARDO-O for this bulky substrate was extremely low, the F275A mutant clearly showed elevated oxygenation activity producing putative *cis*-dihydrodiol from fluoranthene, although the oxygenating site has not been identified. Alanine substitution for the F275 might enlarge the space of the substrate-binding pocket, and this structural change might be beneficial for binding of the bulky aromatic substrate. Similar enlargement of the substrate-binding pocket has been reported in other RO oxygenase components to accommodate larger substrates, such as benzo[*a*]pyrene, benzo[*a*]anthracene, and chrysene.^{19,20)}

His183, His187, and Asp333 coordinate the ferrous iron active site,¹⁰⁾ forming a 2-His-1-carboxylate facial triad (Fig. 4A).²¹⁾ The main chain carbonyl of F329 formed hydrogen bonds to imidazole N^{δ1} of H187.^{10,11)} The F329V mutation can lead to a disorder of the coordination geometry (*viz.*, a distorted octahedral bipyramid) in the CARDO-O active site. This phenomenon can result in the loss of the ferrous iron active site, resulting in negligible or lower activities of F329 mutants. The F329 residue corresponds to the Trp358 residue of the large (α) subunit (the NahAc protein) of the terminal oxygenase component of naphthalene 1,2-dioxygenase (NDO-O) from *Pseudomonas* sp. NCIB9816-4 (Fig. 4A and B). A similar dramatic decrease in oxygenation activity has also been reported for the Ala substitution for W358,²²⁾ although no hydrogen bonding occurred between W358 and the ligand active sites.²³⁾

To the best of our knowledge, the amino acid residues located near the entrance of the active site pocket, such as I262 of CARDO-O, have not been targets of regional design for the alteration of substrate specificities of ROs. This amino acid is located in close proximity to F204 and I231 (Fig. 4A). These amino acid residues are located on the loops, which move to the entrance of the substrate-binding pocket upon carbazole binding.¹¹⁾ These conformational changes presumably result in trapping carbazole at the substrate-binding site and excluding water from the active site during turnover, and prevent the leakage of partially processed substrates. In addition, the *sec*-butyl side chain of I262 forms hydrophobic interactions with the portion of the aromatic ring of the carbazole skeleton in which oxygenation is not occurring (Figs. 2 and 4A). This suggests the possibility that this residue affects not only the orientation of the substrate in the substrate-binding pocket, but also the

introduction of the substrate into the active site cavity or the leakage of substrate/intermediate from the cavity. In fact, the noteworthy changes in substrate specificity due to I262 replacement are improved selectivity and oxygenation activity for anthracene by I262L mutant (Table 2) and increased aromatic-ring hydroxylating activity for dibenzothiophene by I262A and I262W mutants (Table 4).

We have found that the shape of the substrate-binding pocket of CARDO-O is quite different from those of the terminal oxygenase component of other ROs.¹⁰⁾ However, the carbazole-interacting wall consisting of F275, Q282, and F329 in the CARDO-O active site virtually corresponds to the naphthalene-interacting wall, consisting of V260, L307, F352, and W358, in the active site of NDO-O from NCIB9816-4 (all amino acid residues are in the α subunit of the NDO-O molecule; Fig. 4B). Of these residues, F352 is critical in determining both the regio- and enantioselectivity of the enzyme with a variety of substrates.^{22,24)} In nitrobenzene 1,2-dioxygenase from *Comamonas* sp. JS765 and 2-nitrotoluene 2,3-dioxygenase from *Acidovorax* sp. JS42, the amino acid residues corresponding to V260 and F352 in the NDO-O active site are important in determining regiospecificity with nitroarene substrates and enantiospecificity with naphthalene.²⁵⁻²⁷⁾ Suenaga and coworkers²⁸⁻³⁰⁾ performed mutagenesis of the terminal oxygenase component of biphenyl 2,3-dioxygenase (BDO-O) from *Pseudomonas pseudoalcaligenes* KF707 and generated many BDO-O mutants that had different oxygenation activity for polychlorinated biphenyl (PCB) congeners and other aromatic compounds. They found that I335, T376, and F377 in the active site of BDO-O from KF707 are important for regiospecificity with various PCB congeners. These amino acid residues correspond to I326, T367, and F368 respectively in BDO from *Rhodococcus jostii* RHA1, whose crystal structure has been reported.³¹⁾ Superposition of the carbazole-bound structures of CARDO-O¹¹⁾ and biphenyl-bound BDO-O³¹⁾ clearly shows that such important amino acid residues are located in the wall corresponding to F275, Q282, and F329 in the CARDO-O structure (Fig. 4C). Overall, amino acid residues that alter substrate specificity in CARDO-O and those that affect the regio- and stereoselectivity of product formation in the above-mentioned terminal oxygenases lay in similar regions. The observation of many crystal structures of the terminal oxygenase components of ROs indicates that the orientation of substrate binding at the active site is the primary determinant of product regio- and stereoselectivity, as suggested by Ferraro *et al.*³²⁾ These regions tend to form the topology of the active site that influences substrate orientation.

Recently, the structure of the F352V NDO-O mutant was reported as native, phenanthrene-bound, and anthracene-bound forms.³³⁾ This achievement clearly indicated how the Val substitution for F352 affects the substrate orientation in the active site and results in a

change in the regio- and stereoselectivity of product formation. A comparison of the substrate-binding structures of NDO-O with the terminal oxygenase of nitrobenzene 1,2-dioxygenase from *Comamonas* sp. JS765 also indicates the role of amino acid residues, affecting regiospecificity in nitroarene substrate oxygenation and stereoselectivity in naphthalene oxygenation.^{26,27)} Structural information from CARDO-O mutants should help in understanding the role of replaced amino acids in the regulation of substrate orientation. Such detailed studies of the relationship between structure and substrate specificity should provide critical cues to the modification and modulation of the substrate pocket structure to obtain an enhanced catalyst for two distinct areas of scientific endeavor: bioremediation (degradation) of toxic contaminants and enzymatic synthesis of chiral precursors in the production of specialty compounds. In addition, other amino acid residues that possibly interact directly with the substrate, such as I184, L200, A259, V272, and E284 (Fig. 4), are future targets of site-directed mutation to generate CARDO-O mutants that have noteworthy oxygenating activity for various substrates, thus helping to obtain further information on the mechanisms determining the substrate specificity of CARDO.

Acknowledgments

This study was supported by a Grant-in-Aid for Scientific Research (17380052, to HN) from the Ministry of Education, Culture, Sports, Science, and Technology of Japan, and by the Program for Promotion of Basic Research Activities for Biosciences (PROBRAIN).

References

- 1) Boyd, D. R., and Sheldrake, G. N., The dioxygenase-catalyzed formation of vicinal *cis*-diols. *Nat. Prod. Rep.*, **15**, 309–325 (1998).
- 2) Parales, R. E., and Resnick, S. M., Aromatic ring hydroxylating dioxygenases. In "Pseudomonas Volume 4," eds. Ramos, J.-L., and Levesque, R. C., Springer, New York, pp. 287–340 (2006).
- 3) Arcos, J. C., and Argus, M. F., Molecular geometry and carcinogenic activity of aromatic compounds. New perspectives. *Adv. Cancer Res.*, **11**, 305–471 (1968).
- 4) Nojiri, H., and Omori, T., Carbazole metabolism by pseudomonads. In "Pseudomonas Volume 5," eds. Ramos, J.-L., and Filloux, A., Springer, New York, pp. 107–145 (2007).
- 5) Sato, S., Nam, J.-W., Kasuga, K., Nojiri, H., Yamane, H., and Omori, T., Identification and characterization of genes encoding carbazole 1,9a-dioxygenase in *Pseudomonas* sp. strain CA10. *J. Bacteriol.*, **179**, 4850–4858 (1997).
- 6) Nojiri, H., Nam, J.-W., Kosaka, M., Morii, K., Takemura, T., Furihata, K., Yamane, H., and Omori, T., Diverse oxygenation catalyzed by carbazole 1,9a-dioxygenase from *Pseudomonas* sp. strain CA10. *J. Bacteriol.*, **181**, 3105–3113 (1999).

- 7) Nojiri, H., and Omori, T., Molecular bases of aerobic bacterial degradation of dioxins: involvement of angular dioxygenation. *Biosci. Biotechnol. Biochem.*, **66**, 2001–2016 (2002).
- 8) Nam, J.-W., Nojiri, H., Noguchi, H., Uchimura, H., Yoshida, T., Habe, H., Yamane, H., and Omori, T., Purification and characterization of carbazole 1,9a-dioxygenase, a three-component dioxygenase system of *Pseudomonas resinovorans* strain CA10. *Appl. Environ. Microbiol.*, **68**, 5882–5890 (2002).
- 9) Takagi, T., Nojiri, H., Yoshida, T., Habe, H., and Omori, T., Detailed comparison between the substrate specificities of two angular dioxygenases, dibenzofuran 4,4a-dioxygenase from *Terrabacter* sp. and carbazole 1,9a-dioxygenase from *Pseudomonas resinovorans*. *Biotechnol. Lett.*, **24**, 2099–2106 (2002).
- 10) Nojiri, H., Ashikawa, Y., Noguchi, H., Nam, J.-W., Urata, M., Fujimoto, Z., Uchimura, H., Terada, T., Nakamura, S., Shimizu, K., Yoshida, T., Habe, H., and Omori, T., Structure of the terminal oxygenase component of angular dioxygenase, carbazole 1,9a-dioxygenase. *J. Mol. Biol.*, **351**, 355–370 (2005).
- 11) Ashikawa, Y., Fujimoto, Z., Noguchi, H., Habe, H., Omori, T., Yamane, H., and Nojiri, H., Electron transfer complex formation between oxygenase and ferredoxin components in Rieske nonheme iron oxygenase system. *Structure*, **14**, 1779–1789 (2006).
- 12) Sambrook, J., and Russell, D. W., “Molecular Cloning, a Laboratory Manual” 3rd ed., Cold Spring Harbor Laboratory Press, Cold Spring Harbor (2001).
- 13) Nojiri, H., Sekiguchi, H., Maeda, K., Urata, M., Nakai, S., Yoshida, T., Habe, H., and Omori, T., Genetic characterization and evolutionary implications of *car* gene cluster in the carbazole degrader *Pseudomonas* sp. strain CA10. *J. Bacteriol.*, **183**, 3663–3679 (2001).
- 14) DeLano, W. L., “The PyMOL User’s Manual,” DeLano Scientific, San Carlos (2001).
- 15) Inoue, K., Widada, J., Nakai, S., Endoh, T., Urata, M., Ashikawa, Y., Shintani, M., Saiki, Y., Yoshida, T., Habe, H., Omori, T., and Nojiri, H., Divergent structures of carbazole degradative *car* operon isolated from Gram-negative bacteria. *Biosci. Biotechnol. Biochem.*, **68**, 1467–1480 (2004).
- 16) Grifoll, M., Selifonov, S. A., Gatlin, C. V., and Chapman, P. J., Actions of a versatile fluorene-degrading bacterial isolate on polycyclic aromatic compounds. *Appl. Environ. Microbiol.*, **61**, 3711–3723 (1995).
- 17) Kasuga, K., Habe, H., Chung, J.-S., Yoshida, T., Nojiri, H., Yamane, H., and Omori, T., Isolation and characterization of the genes encoding a novel oxygenase component of angular dioxygenase from Gram-positive dibenzofuran-degrader *Terrabacter* sp. strain DBF63. *Biochem. Biophys. Res. Commun.*, **283**, 195–204 (2001).
- 18) Bradford, M. M., A rapid and sensitive method for the quantitation of microgram quantities of protein utilizing the principle of protein dye binding. *Anal. Biochem.*, **72**, 248–254 (1976).
- 19) Ferraro, D. J., Brown, E. N., Yu, C.-L., Parales, R. E., Gibson, D. T., and Ramaswamy, S., Structural investigations of the ferredoxin and terminal oxygenase components of the biphenyl 2,3-dioxygenase from *Sphingomonas yanoikuyae* B1. *BMC Struct. Biol.*, **7**, 10 (2007).
- 20) Jakoncic, J., Jouanneau, Y., Meyer, C., and Stojanoff, V., The catalytic pocket of the ring-hydroxylating dioxygenase from *Sphingomonas* CHY-1. *Biochem. Biophys. Res. Commun.*, **352**, 861–866 (2007).
- 21) Hegg, E. L., and Que, L., Jr., The 2-His-1-carboxylate facial triad: an emerging structural motif in mononuclear non-heme iron(II) enzymes. *Eur. J. Biochem.*, **250**, 625–629 (1997).
- 22) Parales, R. E., Lee, K., Resnick, S. M., Jiang, H., Lessner, D. J., and Gibson, D. T., Substrate specificity of naphthalene dioxygenase: effect of specific amino acids at the active site of the enzyme. *J. Bacteriol.*, **182**, 1641–1649 (2000).
- 23) Kauppi, B., Lee, K., Carredano, E., Parales, R. E., Gibson, D. T., Eklund, H., and Ramaswamy, S., Structure of an aromatic-ring-hydroxylating dioxygenase-naphthalene 1,2-dioxygenase. *Structure*, **6**, 571–586 (1998).
- 24) Parales, R. E., Resnick, S. M., Yu, C.-L., Boyd, D. R., Sharma, N. D., and Gibson, D. T., Regioselectivity and enantioselectivity of naphthalene dioxygenase during arene *cis*-dihydroxylation: control by phenylalanine 352 in the alpha subunit. *J. Bacteriol.*, **182**, 5495–5504 (2000).
- 25) Lee, K.-S., Parales, J. V., Friemann, R., and Parales, R. E., Active site residues controlling substrate specificity in 2-nitrotoluene dioxygenase from *Acidovorax* sp. strain JS42. *J. Ind. Microbiol. Biotechnol.*, **32**, 465–473 (2005).
- 26) Friemann, R., Ivkovic-Jensen, M. M., Lessner, D. J., Yu, C.-L., Gibson, D. T., Parales, R. E., Eklund, H., and Ramaswamy, S., Structural insight into the dioxygenation of nitroarene compounds: the crystal structure of nitrobenzene dioxygenase. *J. Mol. Biol.*, **348**, 1139–1151 (2005).
- 27) Ju, K.-S., and Parales, R. E., Control of substrate specificity by active-site residues in nitrobenzene dioxygenase. *Appl. Environ. Microbiol.*, **72**, 1817–1824 (2006).
- 28) Suenaga, H., Goto, M., and Furukawa, K., Emergence of multifunctional oxygenase activities by random priming recombination. *J. Biol. Chem.*, **276**, 22500–22506 (2001).
- 29) Suenaga, H., Mitsuoka, M., Ura, Y., Watanabe, T., and Furukawa, K., Directed evolution of biphenyl dioxygenase: emergence of enhanced degradation capacity for benzene, toluene, and alkylbenzenes. *J. Bacteriol.*, **183**, 5441–5444 (2001).
- 30) Suenaga, H., Watanabe, T., Sato, M., Ngadiman, and Furukawa, K., Alteration of regioselectivity in biphenyl dioxygenase by active-site engineering. *J. Bacteriol.*, **184**, 3682–3688 (2002).
- 31) Furusawa, Y., Nagarajan, V., Tanokura, M., Masai, E., Fukuda, M., and Senda, T., Crystal structure of the terminal oxygenase component of biphenyl dioxygenase derived from *Rhodococcus* sp. strain RHA1. *J. Mol. Biol.*, **342**, 1041–1052 (2004).
- 32) Ferraro, D. J., Gakhar, L., and Ramaswamy, S., Rieske business: structure-function of Rieske non-heme oxygenases. *Biochem. Biophys. Res. Commun.*, **338**, 175–190 (2005).
- 33) Ferraro, D. J., Okerlund, A. L., Mowers, J. C., and Ramaswamy, S., Structural basis for regioselectivity and stereoselectivity of product formation by naphthalene 1,2-dioxygenase. *J. Bacteriol.*, **188**, 6986–6994 (2006).